Lateral diffusion of an octadecylferrocene amphiphile in Langmuir–Blodgett bilayer assemblies. Effects of the amphiphile concentration

ARTICLE *in* LANGMUIR · AUGUST 1993

Impact Factor: 4.46 · DOI: 10.1021/la00032a043

3 AUTHORS, INCLUDING:

Britta Lindholm-Sethson
Umeå University
36 PUBLICATIONS **560** CITATIONS

SEE PROFILE

Lateral Diffusion of an Octadecylferrocene Amphiphile in Langmuir–Blodgett Bilayer Assemblies. Effects of the Amphiphile Concentration

Britta Lindholm-Sethson,† James T. Orr, and Marcin Majda*

Department of Chemistry, University of California in Berkeley, Berkeley, California 94720

Received February 8, 1993. In Final Form: June 11, 1993

Interdigitated microelectrode array (IMA) devices and steady-state collector–generator voltammetry were used to investigate lateral diffusion processes in bilayer assemblies of octadecyltrichlorosilane (OTS) and octadecylferrocene ($C_{18}Fc$). The OTS monolayer was self-assembled onto glass surfaces in the interelectrode space of the IMA. A Langmuir–Blodgett (L–B) technique was used to transfer Y-type $C_{18}Fc$ monolayers onto OTS-treated surfaces. Variation of the L–B transfer pressure enabled us to control the $C_{18}Fc$ surface concentration in the OTS/$C_{18}Fc$ bilayer in the range of 1.0×10^{-10} to 4.0×10^{-10} mol/cm^2. In this concentration range, the $C_{18}Fc$ lateral diffusion coefficient decreased from 4.8×10^{-8} to 1.7×10^{-8} cm^2/s, reflecting a decreasing fluidity of the monolayer assembly. These results are compared to the measurements on the air/water interface where $C_{18}Fc$ lateral diffusion coefficients were found to be approximately 1 order of magnitude larger. A more condensed nature of the hydrocarbon region, midplane shear interaction, as well as the chain interdigitation in the bilayer assembly are postulated to account for the observed differences in lateral mobility of $C_{18}Fc$ in these two systems.

Introduction

There has been growing interest among chemists in the design, structure, and function of organized molecular assemblies. Microheterogeneous assemblies as diverse in structure and function as those which mimic biological systems,[1–3] perform catalytic functions in solar energy conversion[4] and electroenzymatic catalysis,[5–7] and those designed to work as microelectronic devices[8–10] have been created and investigated. A unifying theme of this large and diverse body of research is the desire to understand structure vs function relationships of synthetic multimolecular systems on the scale of 10–1000 Å. In this range of sizes, classical organic chemistry methods are usually no longer useful as synthetic tools. Thus, new assembly techniques have to be developed which will allow us to fabricate these types of systems with increasing precision and level of molecular complexity.

Research in a number of laboratories has focused on self-assembly and Langmuir–Blodgett techniques as methods to create organized molecular assemblies.[11,12] Our group has often relied on these techniques.[5,13,14] In addition, we have introduced electrochemical methods which allow us to investigate dynamic properties of these types of monolayer structures.[5] Specifically, we have developed the capability of investigating dynamics of lateral diffusion and charge transport in Langmuir monolayers at the air/water interface[15–17] and in self-assembled bilayers at solid/liquid interfaces.[18]

In the latter case, our most recent contribution described fabrication and application of interdigitated microelectrode array (IMA) devices to the measurements of lateral diffusion of electrochemically active amphiphiles in bilayer assemblies.[18] A schematic diagram of an elementary unit of the IMA device with a bilayer assembly is shown in Figure 1. The diagram shows a cross-sectional view of a pair of gold microelectrodes deposited on a glass slide with a bilayer assembled in the interelectrode gap. The pair of gold electrodes represents an array of $N = 100$ interdigitated microelectrodes, each of which is 500 Å in thickness, 800 μm in length, and 4 μm in width with an interelectrode spacing of 4 μm. These devices allowed us to measure lateral diffusion of an amphiphile, *N*-methyl-*N*′-octadecyl-4,4′-bipyridinium dichloride ($C_{18}MV^{2+}$), in the top half of the bilayer under steady-state conditions.[5,18]

From the electrochemical point of view, these measurements involve application of oxidizing and reducing potentials to the alternating microelectrodes that establish steady-state fluxes of the oxidized and reduced amphiphiles between the anode and the cathode of each pair of the microelectrodes of an IMA device. Under such conditions, the steady-state current can be expressed by the following equation[18]

$$i_{ss} = [(N-1)nF\Gamma(l/d)][2D_oD_r/(D_o + D_r)] \qquad (1)$$

where Γ is the surface concentration of the amphiphile in

* To whom all correspondence should be addressed.
† Current address: Department of Analytical Chemistry, Umea University, S-90187 Umea, Sweden.

(1) Ringsdorf, H.; Schlarb, B.; Venzmar, J. *Angew. Chem., Int. Ed. Engl.* **1988**, *27*, 113.
(2) Lehn, J.-M. *Angew. Chem., Int. Ed. Engl.* **1988**, *27*, 89.
(3) Fendler, J. H. *Membrane Mimetic Chemistry*; J. Wiley: New York, 1982.
(4) Hurst, J. K. In *Kinetics and Catalysis in Microheterogeneous Systems*, Surfactant Science Series Vol. 38; Gratzel, M., Kalyanasundaram, K., Eds.; Marcel Dekker: New York, 1991; Chapter 7, p 183.
(5) Majda, M. In *Kinetics and Catalysis in Microheterogeneous Systems*; Surfactant Science Series Vol. 38; Gratzel, M., Kalyanasundaram, K., Eds.; Marcel Dekker: New York, 1991; Chapter 8, p 227.
(6) Parpaleix, T.; Laval, J. M.; Majda, M.; Bourdillon, C. *Anal. Chem.* **1992**, *64*, 641.
(7) Klyachko, N. L.; Levashov, A. V.; Kabanov, A. V.; Khmelnitsky, Y. L.; Martinek, K. In *Kinetics and Catalysis in Microheterogeneous Systems*; Surfactant Science Series Vol. 38; Gratzel, M., Kalyanasundaram, K., Eds.; Marcel Dekker: New York, 1991; Chapter 6, p 135.
(8) Chidsey, C. E. D.; Murray, R. W. *Science* **1986**, *231*, 25.
(9) Wrighton, M. S. *Science* **1986**, *231*, 32.
(10) Fuchs, H.; Ohst, H.; Prass, W. *Adv. Mater.* **1991**, *3*, 10.
(11) Facci, J. S. In *Molecular Design of Electrode Surfaces*; Techniques of Chemistry Series, Vol. 22; Murray, R. W., Ed.; Wiley: New York, 1992; Chapter 3, p 119.
(12) Ulman, A. *An Introduction to Ultrathin Organic Films. From Langmuir–Blodgett to Self-Assembly*; Academic Press: New York, 1991.
(13) Bilewicz, R.; Majda, M. *Langmuir* **1991**, *7*, 2994.
(14) Bilewicz, R.; Majda, M. *J. Am. Chem. Soc.* **1991**, *113*, 5464.
(15) Widrig, C.; Miller, C. J.; Majda, M. *J. Am. Chem. Soc.* **1988**, *110*, 2009.
(16) Charych, D. H.; Landau, E. M.; Majda, M. *J. Am. Chem. Soc.* **1991**, *113*, 3340.
(17) Charych, D. H.; Majda, M. *Thin Solid Films* **1992**, *210/211*, 348.
(18) Goss, C. A.; Majda, M. *J. Electroanal. Chem.* **1991**, *300*, 377.

0743-7463/93/2409-2161$04.00/0

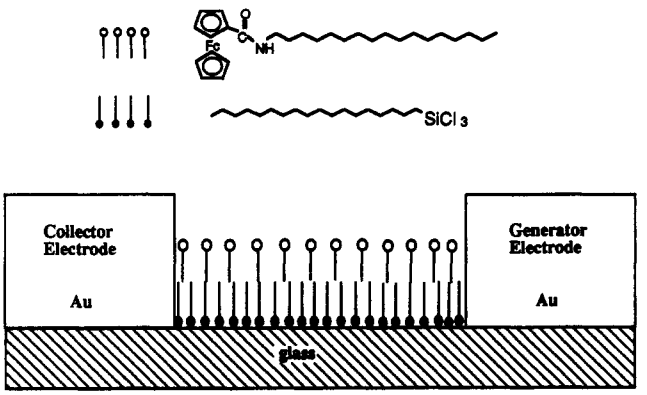

Figure 1. Schematic representation of a bilayer assembly deposited on the glass surface in the interelectrode gap of an interdigitated microelectrode array (IMA) device. The octadecyltrichlorosilane monolayer was formed by self-assembly. Octadecylferrocene monolayer was deposited by the Langmuir–Blodgett technique. IMA is represented here by a cross-sectional view of a single pair of independently addressable electrodes. Actual devices consisted of 50 such pairs of electrodes fabricated by photolithographic techniques. Each electrode was 500 Å thick, 4 μm wide, and 800 μm long. They were spaced by 4 μm (see Experimental Section).

the bilayer assembly, l is the length of each electrode, d is the width of the interelectrode gap, and D_o and D_r are the diffusion coefficients of the oxidized and the reduced forms of the amphiphile. The factor $N-1$ is the number of interelectrode gaps in an array of N microelectrodes. These measurements led us to the elucidation of the effect of charge in the head-group region of an amphiphile on the kinetics of translational diffusion and the structure of the bilayer assembly.[18]

In addition to our fundamental interest in the structure vs function relationship of organized molecular assemblies, the driving force in this research stems from the involvement of the lateral diffusion processes in these types of bilayers in electron transport and charge transfer mediation in electroenzymatic catalysis. Two such applications have been described in the literature where a bilayer assembly involving electroactive amphiphiles, similar to the one described above, was used as a means of enzyme immobilization and also provided the necessary channel of electronic communication between the enzyme molecules and the electrode surface.[6,19]

In this report we rely again on the IMA devices shown schematically in Figure 1 to investigate lateral diffusion processes in bilayer assemblies of nonionic amphiphiles prepared by the Langmuir–Blodgett (L–B) method. Specifically, the bilayer consists of an octadecyltrichlorosilane (OTS) monolayer self-assembled in the interelectrode gap and an L–B monolayer of *N*-octadecylferrocenecarboxamide ($C_{18}Fc$). Our attention is focused primarily on the control of the surface concentration of $C_{18}Fc$ in the L–B monolayer and the effect of that surface concentration on the extent of electroactivity and the rate of lateral diffusion. We discuss these results in relation to our previous studies of diffusivity of charged amphiphiles in self-assembled bilayers[18] as well as in relation to our recent measurements of the translational diffusion of $C_{18}Fc$ at the air/water interface.[16]

Experimental Section

Reagents. *N*-Octadecylferrocenecarboxamide ($C_{18}Fc$) was synthesized by reacting octadecylamine with ferrocenecarboxylic acid and purified by flash chromatography through silica gel as described elsewhere.[16] Octadecyltrichlorosilane (OTS) and (3-mercaptopropyl)trimethoxysilane (MPS) were used as received from Petrarch Systems Inc. Dibenzyl disulfide (DBDS) was obtained from Fluka. Hexadecane (Aldrich, 99%, anhydrous), chloroform (Fisher, spectranalyzed), and methanol (Fisher, spectroscopic grade) were used as received. Water (house-distilled) was passed through a Barnstead Nanopure II purification train. Its resistivity was above 18 MΩ cm.

Au Deposition. Au was vapor-deposited, as previously reported, onto glass slides treated with MPS to improve Au adhesion.[10] In the case of patterned electrodes (type B electrodes), metal masks were used to define the Au area. Glass slides (1 in. × 3 in.) with their entire surface overcoated with Au were used as substrates for the fabrication of microelectrodes.

Microfabrication. The interdigitated microelectrode arrays were patterned in the Microfabrication Laboratory of the University of California at Berkeley, which is a Class 100 clean room. A film of Au, approximately 60 nm thick, was deposited on the MPS-treated glass slides in a Veeco Model 7700 bell jar under conditions previously described. The Au (99.9%) was from Lawrence Berkeley Laboratory. We used standard photolithographic techniques with photoresist (Shipley 1400-31) and a chrome-patterned glass mask (JTO2) designed with the KIC system on the Microfabrication Laboratory computers. The microelectrode array pattern consisted of two contact pads (4 mm × 3 mm), which functioned as electrical leads. They were 100 μm in width and were gradually narrowed to 25 μm until they reached the array of microelectrodes. The array consisted of 50 pairs of interdigitated microelectrodes. Members of each pair of the microelectrode bars originated from opposite leads of the device. The bars were 800 μm long, 4 μm wide and were separated by 4 μm wide gaps. The other details of the fabrication process were identical to those reported previously.[18]

Self-Assembly of OTS + DBDS. We followed the recipe of Sagiv in the self-assembly of OTS, with only minor modifications.[21-23] One modification was the addition of a small amount of dibenzyl disulfide (DBDS) in order to ensure the existence of a sufficient population of pinholes in the OTS monolayer. We successfully used this method earlier.[18] The addition of DBDS (about 0.5 mol % with respect to OTS) changed the advancing contact angles of droplets of hexadecane and water (see Table I in Results and Discussion). In all experiments, we only used substrates with advancing contact angles of water droplets of more than 90°, and usually over 100°. The addition of DBDS was not necessary when treating IMA electrodes, as a sufficient pinhole density existed in the OTS monolayers at the edges of the microelectrode bars. The other modification was that the glass/Au substrates were immersed twice in the assembly solution, for 7 min each time, and rinsed with chloroform each time when removed from the self-assembly solution and dried with an Ar jet.

Langmuir–Blodgett Techniques. The Langmuir–Blodgett transfers and the subsequent electrochemistry were carried out in a 45 cm × 15 cm Teflon Langmuir trough (KSV Model 2200). Surface pressure was monitored with a Wilhelmy plate (20 mm × 15 mm filter paper) and a microbalance. The operation of the trough was controlled with a PC AT type computer with KSV Dynamic Film Control System Software Version 2.0. The trough, the movable barrier, and the microbalance assembly were enclosed in a large Plexiglas box. All electrical cables, the tubing for aspiration of the subphase, and the gas inlet were brought into the box through Swagelok fittings. Manual access was possible through iris ports. Hands were never allowed in the Plexiglas box unless covered with long length powder-free vinyl gloves (Oak Technical). The box was continuously purged with house nitrogen passed through a 10 nm Matheson membrane gas filter. The humidity in the box was controlled by adjusting the flow rate of nitrogen.

The trough was scrupulously cleaned before use. The Teflon surface was wiped with chloroform (Spectranalyzed) and then with methanol (Spectroscopic Grade) and finally rinsed thoroughly with pure water. In each case the wiping was done with

(19) Bourdillon, C.; Majda, M. *J. Am. Chem. Soc.* **1990**, *112*, 1795.
(20) Goss, C. A.; Charych, D. H.; Majda, M. *Anal. Chem.* **1990**, *63*, 85.
(21) Sagiv, J. *J. Am. Chem. Soc.* **1980**, *102*, 92.
(22) Netzer, L.; Iscovici, R.; Sagiv, J. *Thin Solid Films* **1983**, *100*, 465.
(23) Maoz, R.; Sagiv, J. *J. Colloid Interface Sci.* **1984**, *100*, 465.

lint-free tissues (Techni-Cloth by Texwipes Co.). When a subphase solution was introduced into the trough, the surface was compressed and swept and aspirated with a micropipet. This was repeated several times. There was no increase in surface pressure when the surface of the pure subphase was compressed.

Monolayers of $C_{18}Fc$ were prepared by spreading aliquots of a chloroform solution of $C_{18}Fc$ (about 2 mM) dropwise onto the entire surface of the subphase. The volume of the aliquot was adjusted to deliver 4.5×10^{16} molecules of $C_{18}Fc$, and the initial mean molecular area was about 100 Å^2/molecule. Typically, the aliquots were 35 μL and the trough area during spreading was 450 cm^2. After waiting a few minutes for the chloroform to evaporate, the monolayer was compressed by moving the barrier at a rate of 3 cm/min. This corresponds to a compression rate of 10 (Å^2/molecule)/min.

The above procedure was followed for recording pressure–area isotherms and for performing Langmuir–Blodgett transfers. However, if a transfer was to be carried out, an OTS-treated substrate was positioned approximately 1 cm above the air/water interface before a monolayer was spread onto the subphase. Care was taken to position the substrates perpendicular to the barrier as well as to the surface of the subphase. Monolayers were compressed until the surface pressure reached the desired level for the transfer. The control unit automatically slowed the barrier and moved it as necessary to maintain the desired surface pressure. At this point, we waited about 5 min for the barrier motion to be close to 0 cm/min before beginning the L–B transfer experiment. The residual barrier motion rate was recorded and used to correct the transfer ratio data. The substrates were lowered at a rate of 1 cm/min in a constant surface pressure mode. Our calculation of the mechanical transfer ratio was based on a plot of the barrier position vs time before, during, and after transfer. No difference in the mechanical transfer ratio was found when all Au or all-glass substrates were used.

Electrochemical Experiments. All electrochemical experiments were carried out in the trough after the L–B transfers with the subphase solution acting as the supporting electrolyte. The counter electrode (Pt wire) and reference electrode (SCE) were kept behind a barrier so that they were immersed in the subphase solution but were not in contact with the surface monolayer. Cyclic voltammograms were performed with a locally constructed Model 852 low current bipotentiostat (R. Ensman, Indiana University). These were recorded with a Kipp and Zonen X-Y-Y′-t recorder. For the generator–collector experiments, the generator electrode was ramped from 0 V to 0.8 V (vs SCE) at a rate of 20 mV/s while the collector was held at 0 V (vs SCE). Current was recorded from both electrodes. Chronocoulometric experiments were done with a BAS 100A potentiostat (Bioanalytical Systems Inc.).

Contact Angle Measurements. Advancing contact angles of droplets of water and hexadecane were measured with a Ramè-Hart Model 100 contact angle goniometer. The sessile drops were exposed to laboratory atmosphere.

Results and Discussion

Electroactivity of $C_{18}Fc$ Langmuir–Blodgett Films in Bilayer Assemblies. Figure 2 shows two isotherms (T = 22 °C) of $C_{18}Fc$ spread on a 1.0 M $HClO_4$ subphase in equilibrium with air at different levels of relative humidity. The limiting area obtained by extrapolation of the first segment of increasing pressure was 50 ± 1 Å^2/molecule. This value is independent of the level of water vapor in the air contacting the surface monolayer. The pressure of the broad transition region increased from ca. 18 to 32 mN/m as the relative humidity increased from 10% to 35%. We believe that this behavior reflects an increased stability of the monolayer above 35% humidity level. Further increase of the air humidity had no effect on the pressure of the transition region until the relative humidity was increased above 85% when it resulted in a decrease of the pressure of the transition region and led to instability of the surface monolayer. The most incompressible region of the isotherm at high surface pressures gave the limiting area of 19 ± 2 Å^2/molecule.

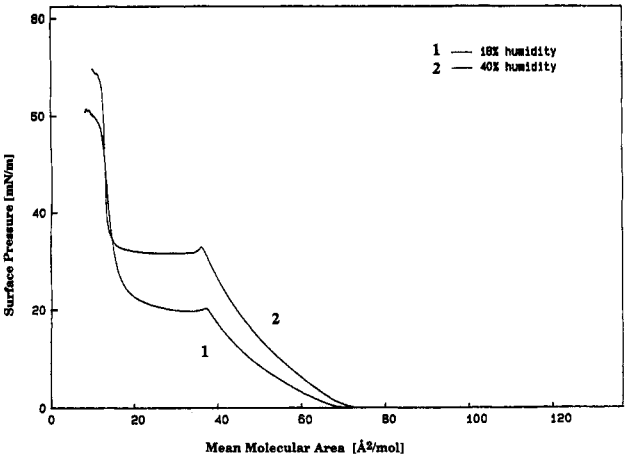

Figure 2. Pressure–area isotherms of $C_{18}Fc$ monolayers recorded on 1.0 M $HClO_4$ subphase under 18% (curve 1) and 40% (curve 2) relative humidity at 22 °C.

These data suggest that the surface monolayer is in a liquid state in the region of surface pressures immediately following a take-off point. The limiting area extrapolated from this region corresponds to the cross-sectional area of the ferrocene head group. Our 2-D electrochemical experiments carried out at the air/water interface confirmed the liquid nature of the $C_{18}Fc$ monolayer in this region.[16] The origin of the transition region is not exactly clear. It is likely due to staggering of the head groups so that the cross-sectional area of the hydrocarbon chains is determining the projected size of the molecules. The experiments described below were carried out at 40% relative humidity. The choice of 1 M $HClO_4$ subphase was dictated by the instability of the ferrocenium cation head group in solutions of lower perchloric acid concentration.

$C_{18}Fc$ Langmuir monolayers showed good stability on the water surface even at appreciable surface pressures approaching the transition region in the π/A isotherm. Following compression of the $C_{18}Fc$ monolayer to any pressure between 0 and 20 mN/m and holding the barrier motion did not lead to pressure decrease in excess of 10% in 40 min. In order to measure the transfer ratio (the ratio of the surface area of substrate crossing the Langmuir monolayer to the decrease of the surface area of the Langmuir monolayer on the water surface) and its dependence on the surface pressure, we carried out L–B transfer of single Y-type $C_{18}Fc$ monolayers onto large 1 × 3 in.^{2} OTS-coated glass slides (glass/OTS). The results are shown in Figure 3. A unit transfer ratio was obtained at all pressures except those close to the pressure of the transition region. The lower values of the transfer ratio at 25 and 29 mN/m could be a result of an error in assessing a steady-state background value of the barrier motion at these pressures. The same results were obtained when gold-coated glass slides with self-assembled OTS layers (Au/OTS) were used.

Besides the geometric transfer ratio, we were also interested in determining the extent of electroactivity of L–B $C_{18}Fc$ monolayers on Au/OTS substrates as well as in the range of surface concentrations that can be covered using the L–B technique as the method of bilayer preparation. Considering the fact that self-assembly of an OTS monolayer may passivate the electrode surface, we first examined the extent of electroactivity of $C_{18}Fc$ L–B monolayers on the OTS-coated gold electrodes. In

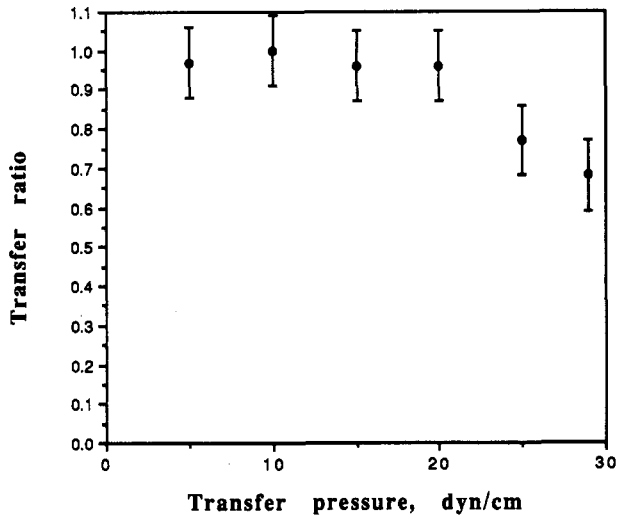

Figure 3. Plot of the transfer ratio vs surface pressure for the L–B transfer of $C_{18}Fc$ monolayers from 1.0 M $HClO_4$ subphase onto OTS-treated glass slides.

these experiments 0.4 cm^2 gold electrodes produced by vapor deposition of gold on glass slides were used. We found that there exists a correlation between the extent of electroactivity of $C_{18}Fc$ in the Au/OTS/$C_{18}Fc$ bilayer and the water contact angle on the Au/OTS surface, measured before the L–B transfer of the $C_{18}Fc$ monolayer. Poorly defined cyclic voltammograms were obtained when the water contact angle was above 112°. Lower contact angles (105–110°), indicating a less well ordered structure of the OTS monolayer, corresponded with well-developed current–voltage curves suggesting full electroactivity. In order to control the permeability of the OTS monolayer and to ensure full electroactivity of $C_{18}Fc$ independent of the OTS structure, the OTS self-assembly was carried out in the presence of 0.5 mol % of dibenzyl disulfide (DBDS). The latter reagent coadsorbs on gold and its presence in the OTS monolayer prevents electrode passivation.[18] It appears that individual DBDS sites act as centers of electroactivity on the electrode surface. At these sites, $C_{18}Fc$ molecules can access the electrode surface at distances sufficiently small to allow electron transfer. If the population density of these sites is large enough and if the time scale of voltammetric experiments is sufficiently long, lateral diffusion of $C_{18}Fc$ to the DBDS sites may account for full electroactivity of the $C_{18}Fc$ molecules. Bell-shaped voltammograms characteristic for systems with surface confined electroactive species were observed. Integration of the current yielded surface concentrations of $C_{18}Fc$ independent of scan rate in the range of 10–100 mV/s and consistent with the amount of $C_{18}Fc$ transferred from the water surface. Lower $C_{18}Fc$ coverage values (by 10–20%) were obtained electrochemically when the scan rate was increased to 200 mV/s, suggesting that the lateral diffusion of $C_{18}Fc$ is indeed one of the steps involved in electroactivity in OTS/$C_{18}Fc$ bilayers.

The effect of DBDS coadsorption on the contact angles of water (θ_{H_2O}) and hexadecane (θ_{Hex}) on OTS/DBDS monolayers on gold is shown in Table I. Knowing that θ_{H_2O} on OTS/DBDS monolayers on gold electrodes used in our experiments was typically 102°, the mole fraction of DBDS in the surface monolayer can be estimated, based on the Cassie equation, to be 0.17.[24] These electrodes showed no passivation effects either in the experiments involving solution species such as $Ru(NH_3)_6^{3+}$ (in 0.1 M KCl electrolyte) or in the experiments involving $C_{18}Fc$ L–B monolayers. As one might expect, the presence of DBDS in the OTS self-assembly solution had no effect on the OTS self-assembly on the glass surface since the former reagent interacts exclusively with gold. The water contact angle on OTS-coated glass slides was 113° while θ_{Hex} ranged, for the same surfaces, from 41° to 45° indicating a larger sensitivity of θ_{Hex} compared to θ_{H_2O} to the structural order of self-assembled OTS monolayers. The use of DBDS co-self-assembly was not necessary on the IMA devices. It appears that the number of defects in the OTS monolayer present on the edges of the interdigitated microelectrodes was sufficient to induce full electroactivity of $C_{18}Fc$.

Table I. Advancing Contact Angles of Water and Hexadecane on Gold Surfaces Coated with Self-Assembled OTS and DBDS Monolayers

mol % DBDS[a]	θ_{H_2O}	θ_{Hex}
0	113	44
0.1	113	44
0.15	106	41
0.2	104	38
0.5	102	34
5	85	10
10	87	9

[a] Mol % of DBDS with respect to OTS in the self-assembly solution in which OTS concentration was 2.0 mM in mixture of hexadecane, chloroform, and carbon tetrachloride.

In order to measure the quantity of $C_{18}Fc$ transferred by the L–B method onto the IMA device surface, voltammetric assay was carried out. In those experiments, both sets of the microelectrodes were driven at a common working electrode potential. The schematic diagram of the OTS/$C_{18}Fc$ bilayer assembled on the surface of an IMA device in Figure 1 presents a simplified picture. In reality, the self-assembly of OTS and L–B transfer of $C_{18}Fc$ result in monolayer and then bilayer formation on the surface of the entire device which includes both the surface of gold microelectrodes and the glass surface in the interelectrode gaps. (Considering the geometry of the IMA devices, the ratio of the gold to glass surface areas is approximately 1.) Knowing that the geometric transfer ratio of $C_{18}Fc$ onto glass/OTS and glass/Au/OTS + DBDS are the same, we calculated the surface concentration of $C_{18}Fc$ (Γ) by simply dividing the quantity of the octadecylferrocene obtained by integration of the cyclic voltammetric current above background (see Figure 6A), by the total surface area of gold and glass of the IMA devices.

The charge due to the oxidation/reduction of $C_{18}Fc$ obtained in the voltammetric assay experiments with IMA devices depended on the scan rate as shown in Figure 4. Also, the shape of voltammograms in these experiments showing some diffusive "tailing" indicated at least partial diffusion control of the redox processes at higher scan rates. This is not unexpected as electroactive material present in the interelectrode gaps has to diffuse as much as 2 μm (half of the interelectrode spacing) in order to become oxidized and/or reduced. On the basis of the data presented in Figure 4, we used a scan rate of 20 mV/s in voltammetric assay experiments. Results from a series of such experiments are shown in Figure 5 demonstrating the capabilities of the L–B methods to vary the surface concentration of amphiphile transferred at various surface pressures. We take advantage of this capability to investigate the effect of $C_{18}Fc$ surface concentration on its lateral diffusion coefficient in the next section.

Lateral Diffusion; Generator/Collector Voltammetry. Thorough discussion of the application of IMA

(24) Cassie, A. B. D. *Discuss. Faraday Soc.* **1948**, *3*, 11.

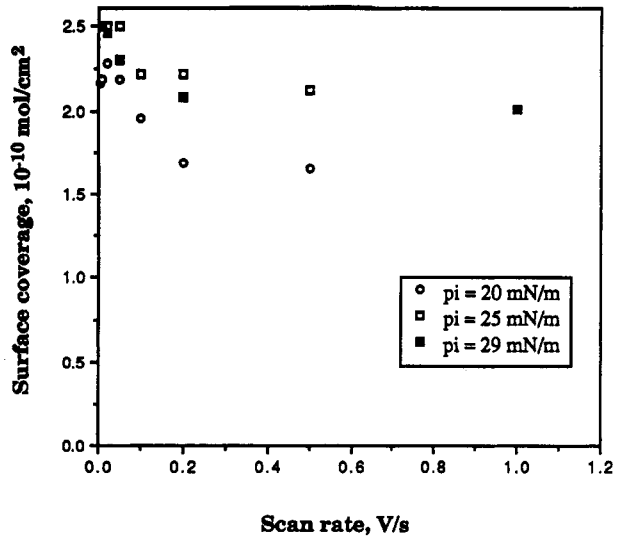

Figure 4. Plots of the electrochemically determined surface coverage of $C_{18}Fc$ in OTS/$C_{18}Fc$ bilayers deposited on IMA devices at different transfer pressures (shown in the figure) vs scan rate of the cyclic voltammetric runs.

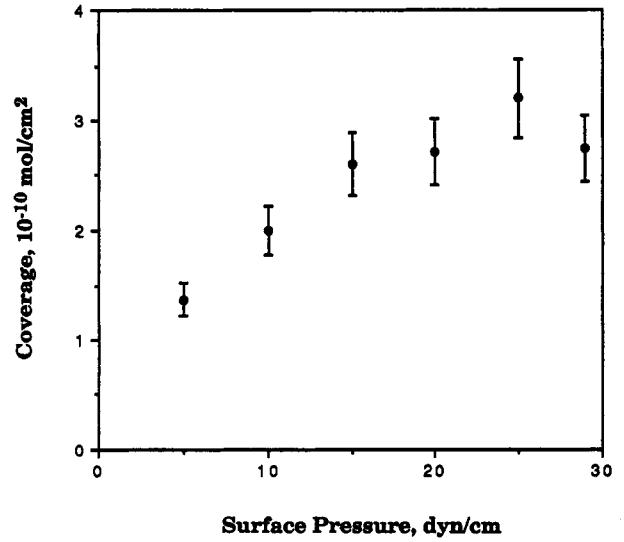

Figure 5. Plot of the surface coverage of $C_{18}Fc$ in OTS/$C_{18}Fc$ bilayer assembly deposited on an IMA device vs L–B transfer pressure. Coverages were measured by voltammetric assay at 20 mV/s.

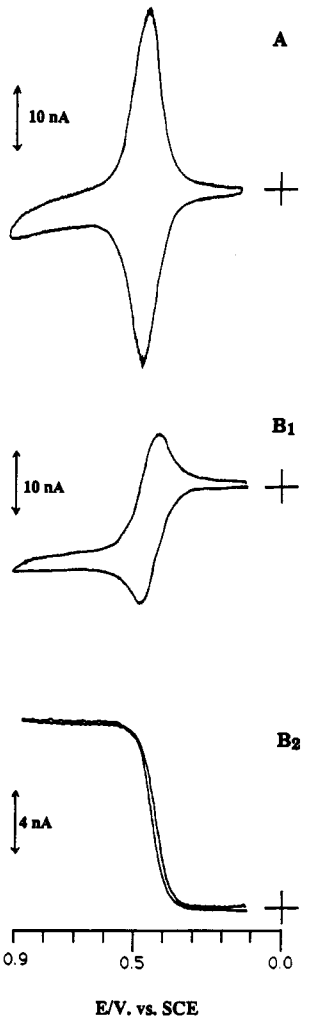

Figure 6. (A) Cyclic voltammogram of $C_{18}Fc$ in a OTS/$C_{18}Fc$ bilayer on an IMA device. The experiment was carried out in a three-electrode potentiostatic mode with both sets of electrodes of the IMA device driven at the common working electrode potential, 1.0 M $HClO_4$, υ = 20 mV/s. (B) Generator/collector voltammograms of the system described in part A carried out in a four-electrode bipotentiostatic mode with the generator electrode scanned from 0.0 to 0.9 V and the collector electrode held at +0.1 V, υ = 20 mV/s. (B_1) generator current–voltage curve. (B_2) collector current recorded at +0.1 V and plotted vs the potential of the generator electrode.

devices to the measurements of the lateral diffusion of amphiphiles in bilayer assemblies has been given in our previous paper in this series.[18] Briefly, one relies on the steady-state generator/collector current which is observed when the potential of one set of microelectrodes of an IMA device is made oxidizing and the other interdigitated set is made reducing with respect to the formal redox potential of the electroactive amphiphile (see Figure 6 and related discussion below). The limiting steady-state current, observed when the concentrations of the oxidized and reduced forms of the amphiphile are zero at the cathode and the anode, respectively, can be described in view of Fick's first law fluxes to the microelectrodes. This yields eq 1.

Equation 1 becomes particularly useful when the diffusion coefficients of both reduced and oxidized species are the same. In such a case, the second term in brackets in eq 1 becomes simply D_{app}. We showed in our earlier studies of octadecylviologen ($C_{18}MV^{2+}/C_{18}MV^{+}$) bilayers that the magnitude of charge in the head group region of the amphiphile, which depends, naturally, on its oxidation state, has a profound effect on the diffusivity of the amphiphile as well as on the fluidity of the monolayer assembly.[18] In the case of $C_{18}MV^{2+}$, D_{ox} was 7 times higher than D_r. In the present case, however, one should not expect big differences in the diffusion coefficient of the two redox states of $C_{18}Fc$ since neither state is charged. Strong ion-pairing of $C_{18}Fc^{+}$ with perchlorate ions in 1 M $HClO_4$ electrolyte neutralizes the charge of $C_{18}Fc^{+}$. Confirmation of this hypothesis was obtained in a series of chronocoulometric experiments in which we applied a large positive or negative potential pulse to a fully reduced or fully oxidized bilayer, respectively. In the short time regime (ca. 1–50 ms) the system evolves under semiinfinite diffusion conditions. Hence, the initial slope of the Anson plots is proportional to the square root of the diffusion coefficient of the species present at the beginning of the experiment. In a series of such experiments we found that D_{ox} equals D_r within the experimental error. Specifically, at $\Gamma_{C_{18}Fc} = 2.4 \times 10^{-10}$ mol/cm^2 $D_{ox} = (3.2 \pm 0.83) \times 10^{-8}$ cm^2/s and $D_r = (2.3 \pm 0.28) \times 10^{-8}$ cm^2/s and at $\Gamma_{C_{18}Fc} = 2.6 \times 10^{-10}$ mol/cm^2 $D_{ox} = (2.9 \pm 1.3) \times 10^{-8}$ cm^2/s and $D_r = (2.4 \pm 0.58) \times 10^{-8}$ cm^2/s. In view of the large

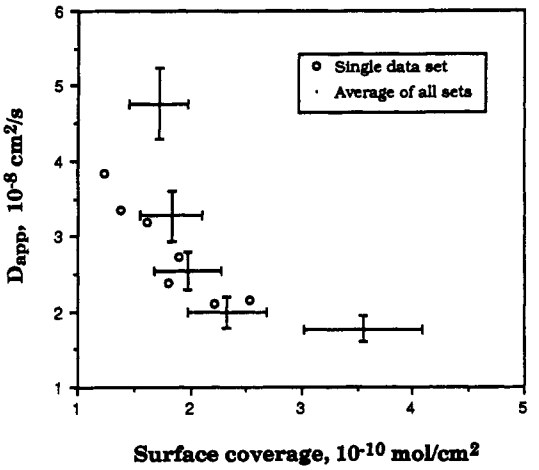

Figure 7. Plot of the $C_{18}Fc$ lateral diffusion coefficient in OTS/$C_{18}Fc$ bilayer assembly vs $C_{18}Fc$ surface concentration. Open circles are a representative single data set. The remaining data represent the averages and standard deviations of seven runs carried out on different IMA devices.

differences between the diffusion coefficients of $C_{18}MV^{2+}$ and $C_{18}MV^{+}$ mentioned above, this result substantiates our notion of strong ion-pairing between ClO_4^- and $C_{18}Fc^+$ species.

Figure 6B shows a set of typical generator/collector voltammograms obtained with the OTS/$C_{18}Fc$ bilayer spanning the interelectrode gap of an IMA device. In such an experiment, generator and collector electrodes are initially held at a reducing potential. At the beginning of the experiment, the potential of the generator electrode is scanned at 20 mV/s in the positive direction while the collector's potential continues to be held at the initial value. The generator current is initially higher than the corresponding collector current in that it contains a significant non-steady-state component. As $C_{18}Fc^+$ species generated at the anode diffuse across the interelectrode gap to the collector, the collector current increases and assumes a steady-state value when the potential of the generator electrode becomes sufficiently positive to generate the maximum flux of oxidized species. Figure 6A shows a cyclic voltammogram recorded with both sets of electrodes driven at the same potential. Integration of current in such experiments served to measure the surface concentration of $C_{18}Fc$ species before and after each steady-state run.

The dependence of the lateral diffusion coefficient, D_{app}, on the surface concentration of $C_{18}Fc$ in the bilayer is shown in Figure 7. Open circles mark a representative set of data obtained with a single IMA device. In such a series of experiments, each L–B transfer carried out at a particular surface pressure was followed by a voltammetric assay, steady-state generator/collector experiment, and one more voltammetric assay. The average value of coverage obtained in both voltammetric assay experiments was used to evaluate the steady-state generator/collector data. Subsequently, the $C_{18}Fc$ monolayer was rinsed off with chloroform and the OTS-coated IMA device was used in the next L–B transfer experiment at a different surface pressure. When different IMA devices are used in such experiments, somewhat different values of diffusion coefficient are observed at the same surface concentrations of $C_{18}Fc$. These variations are probably related to small differences in the structure of OTS monolayers and to the differences of the individual IMA devices. The D_{app} vs Γ plot obtained by averaging all the data from seven different devices is also shown in Figure 7.

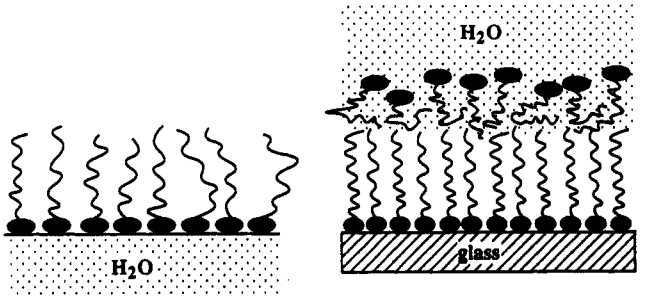

Figure 8. Schematic representation of the $C_{18}Fc$ monolayer at the air/water interface and OTS/$C_{18}Fc$ bilayer assembly on the surface of an IMA device in water.

The decreasing character of the D_{app} vs Γ curve reflects the decreasing fluidity of $C_{18}Fc$ monolayers with increasing concentration of the amphiphile. The same trend was observed in the behavior of this amphiphile at the water surface.[16] In those experiments, we showed direct proportionality of D to the average free area per molecule on the water surface. Such behavior was shown to be consistent with a model of diffusion of hard sphere fluids.[25-27] The same proportionality can be found in the behavior of $C_{18}Fc$ bilayer assemblies. More important, however, is the comparison of the absolute magnitudes of the diffusion coefficients of $C_{18}Fc$ on the water surface and in bilayer assemblies on OTS at the same concentrations of the ferrocene amphiphile. Both systems are depicted schematically in Figure 8. By making such a comparison, we find that $C_{18}Fc$ lateral diffusion in the bilayer assembly is an order of magnitude slower than its diffusivity on the water surface. Considering the nature and the differences of the two systems, it becomes apparent that the structure of the hydrocarbon region of the bilayer and the extent of interactions between the alkyl chains of the OTS and $C_{18}Fc$ monolayers play a crucial role in setting the value of D_{app} measured in the experiments discussed above. Of particular importance in these interactions are such elements as the degree to which the $C_{18}Fc$ monolayer is collapsed onto the OTS monolayer, which determines the magnitude of shear interactions. The structure of the OTS monolayer is also a factor in that in may affect the extent of intercalation of the hydrocarbon chains of the two amphiphiles. In general, D_{app} reflects the fluidity of the hydrocarbon region of the OTS/$C_{18}Fc$ bilayer. In contrast to these types of effects and interactions, diffusion of $C_{18}Fc$ at the air/water interface was shown to be largely limited by the interactions within the head-group region and by weak coupling of the ferrocenecarboxamide moiety to the aqueous subphase.[16]

In the studies of the $C_{18}MV^{2+}/C_{18}MV^{+}$ system, we showed that the extent of collapse of the octadecylviologen monolayer onto the OTS sublayer was closely related to the formal charge in the head-group region.[18] Progressive reduction of $C_{18}MV^{2+}$ decreased its diffusion coefficient from 7.5×10^{-8} to 1.5×10^{-8} cm^2/s (see Figure 18 in ref 18 and the related discussion). Comparing these values with D_{app} reported above for the $C_{18}Fc$ system, one may conclude that the extent of collapse of the latter monolayer is similar to the 70% reduced $C_{18}MV^{2+}/C_{18}MV^{+}$ system. (This comparison was made at the same surface concentration for the two bilayer systems.) In the latter case, the experiments were done in 1 M KCl electrolyte where

(25) Cohen, M. H.; Turnbull, D. *J. Chem. Phys.* **1959**, *31*, 1164.
(26) Turnbull, D.; Cohen, M. H. *J. Chem. Phys.* **1970**, *58*, 3038.
(27) Beck, K. In *Cytomechanics. The Mechanical Basis of Cell Form and Structure*; Bereiter-Hahn, J., Anderson, O. R., Eds.; Springer Verlag: Berlin, 1987; Chapter II.1, p 79.

substantial ion pairing of both $C_{18}MV^{2+}$ and $C_{18}MV^{+}$ decreased their formal charge. Thus, it becomes clear that the fluidity and diffusivity in bilayer assemblies depend on the surface density of the amphiphiles as well as on the effective charge in the head-group region. Other factors affecting fluidity of bilayer assemblies, such as length and type of hydrocarbon chains and type of contacting electrolyte, were kept invariant in the investigations discussed above. The data presented in this report demonstrate also the usefulness of the Langmuir–Blodgett technique in building monolayer structures of controlled composition and surface concentration.

Acknowledgment. We acknowledge and thank the National Science Foundation for supporting this research under Grant CHE-9108378. B.L.-S. also acknowledges financial support from the Swedish Natural Science Research Council and the Sweden–America Foundation during her visit in Berkeley.